TIME INTEGRATED X-RAY MEASUREMENTS OF THE VERY ENERGETIC ELECTRON END LOSS PROFILE IN TMX-U

J. E. Osher and J. Fabyan
Lawrence Livermore National Laboratory, University of California
Livermore, CA 94550

UCRL--91507
DE85 001567

ABSTRACT

The time-integrated 2-D profile of the thick-target bremsstrahlung produced by energetic end loss electrons has been measured during ECRH operation of TMX-U. Sheets of x-ray film and/or arrays of thermoluminescent dosimeters were placed on the outside of the end tank end wall to measure the relative spatial x-ray profile, with locally added filters of Pb to determine the effective mean x-ray energy. The purpose of this simple survey diagnostic was to allow deduction of the gross features of the ECRH region. The electron source functions needed to fit the x-ray data were modeled for various anchor cell radial distributions mapped along magnetic field lines to the elliptical plasma potential control plates or the Al end walls. The data are generally consistent with (1) major ECR heating in the central 25-cm-diam core, (2) a mean ECRH electron loss energy of 420 keV, and (3) an ECRH coupling efficiency to these hot electrons of $\geq$10%.

INTRODUCTION

Tandem mirror machines with thermal barriers[1] require local production of very hot electron populations in the end plug regions to attain high efficiency. The radial profile of these very energetic (several hundred keV)

electrons produced by electron-cyclotron resonant heating (ECRH) is of interest for evaluating the heating efficiency and radial density profile in the Tandem Mirror Experiment-Upgrade (TMX-U). The purpose of the simple diagnostic of this paper was to make a relatively quick survey of the hot ECRH electrons with minimal equipment and without special internal access and so to help plan for more elaborate time resolved measurements. Our approach was to place sheets of x-ray film and/or an array of thermoluminescent dosimeters on the external TMX-U end wall to record an approximate time-integrated 2-D image of the thick target bremsstrahlung produced by end loss ECR heated electrons impinging on the inside of the end wall.

The limitations of this technique include: (1) the exposure is time-integrated over the entire duration of a shot (or set of shots), (2) there is the assumption that the energetic electron loss profile is simply related by magnetic mapping to the ECRH region, and (3) that the penetrating x-ray radiation producing the specific 2-D exposure is a sufficiently representative sample in space and energy to guide modeling of the ECRH process. As a further limitation in TMX-U, the central core of electrons maps to elliptical plasma-potential-control (PPC) plates located approximately 50 cm in front of the detection plane rather than just on the back side of the detector plane, preferable for maximum spatial resolution. Only for the first measurement does the outer portion of the electron loss map to the back side of the 2.54-cm-thick access door adjacent to the film plane. The argument that the principal energetic electron loss occurs only during the ECRH time rather than during the observed long, low density, hot electron afterglow decay is described in Sec. II.

I. EXPERIMENTAL ARRANGEMENT

We measure the end loss using the two detector types under two somewhat different machine geometries and machine operating conditions.

Case 1

The first measurement was made using two 14-in. x 17-in. x-ray film cassettes located over an access port with only a 2.54-cm-thick Al door on the TMX-U west end tank wall (wall nominally 7.3-cm-thick Al). The geometry for this exposure is shown in Figs. 1a and 1b. Note that the exposure was approximately 1 m off the minor axis of the ellipse, with one cassette above the plane of the major axis and one below to check for symmetry. The central elliptical PPC plate and the elliptical annular guard ring were located approximately 50 cm from the end wall, as shown in the figures. The exposure was made over essentially one good shot with a high diamagnetic signal. Strips of 1/16-in.-thick Cu and 1/8-in.-thick Pb were added to adjust the exposure level for a wider range of readability. The exposure with only one good shot was such to make the type X-OMAT film with a $CaWO_4$ intensifier screen somewhat over-darkened except behind the Cu and Pb shadow strips.

Case 2

Our second measurement was made with an array of some 50 dosimeters located along both the major and minor axes of the west end fan, and along a chord set 1 m from the minor axis. In addition two detectors were placed on

the east end fan to check for east-west symmetry. The machine end geometry for the case 2 exposure was changed from case 1 in that the end-loss electrons now impinged on a larger sized coaxial set of five PPC (or annular elliptical) plates located from 50 to 70 cm from the tank wall. Also for case 2 the machine was just being worked up with generally much lower diamagnetic signals. The exposure for this case was made over approximately 10 good shots during a high gas flow scan. A separate array of dosimeters and various thicknesses of Pb were placed near the machine axis just outside the 7.3 cm thick west end wall to measure the average penetrating x-ray energy.[2]

II. DATA ANALYSIS

For Case 1 the x-ray film was read out with a precision densitometer scan yielding x-ray intensity vs scan position at various selected film locations. A scan along X (the major axis) across the Cu and Pb strips was used for an x-ray attenuation fit to yield a mean penetrating x-ray energy of approximately 350 keV for the exposure of Case 1. Also, the X-OMAT film with $CaWO_4$ intensifier screen (as used for chest x-rays) was calibrated at the LLNL X-ray facility against standard dosimeters, indicating an x-ray intensity at the film plane of approximately 25 mrem/shot. The x-ray intensity vs Y scan for the selected X axis (major axis) positions of the two strips (both oriented along the Y axis) were then plotted as data input. These were compared to calculated intensity yields from various x-ray source functions modeled from axially symmetric ECRH electron distributions in the anchor midplane mapped along magnetic field lines to impact either on the elliptical PPC plates or on the inside of the access door. The results for the source

function needed to best fit the experimental scan behind the Cu strip is illustrated in Fig. 2a. The lower dashed line shows a "good fit" of the model x-ray source strength vs Y. The total x-ray yield from the central plates is well determined, but the radial model resolution is very poor. Figure 2b depicts the same data without the PPC plate contribution for comparison. The solid line in each case shows the normalized exposure calculated from the 3-D source integration, corrected for attenuation in the various interposed materials between the source element and the film. Finally, the dot-dot-dash curve shows the experimental data curve. The x-ray radiation from each element of the 2-D integration over the elliptical source area was taken as isotropic. The relativistic forward peaking correction at 350 keV is only a few percent for x-rays over $\pm 25^{0}$ forward angles and able to penetrate the thick walls. The larger front-to-back integrated ratio was included in calculating the electron flux required for the observed yield. A good match of the data to the model calculation requires that the main x-ray source ($\sim$85%) comes from the central PPC plates that magnetically map to the 20-cm-diam core in the anchor midplane. The remaining 15% is either contributed by ECRH electrons produced in the outer halo or produced from scattering during the long, low density, hot electron tail (τ > 30 s) as the magnetic field decays (τ = a few seconds). This, in turn, sweeps the magnetic field lines outward and probably most of the hot electrons into the limiter. A small 1-cm-thick rim of electrons just outside of the control plates improves the model fit to the data, however no complete fit was found, unless one includes sufficient radial diffusion of the hot ECRH electrons while the ECRH is on. This diffusion could partially fill the source gap shown from 12 cm to 20 cm along Y due to magnetic field line divergence over

the 50 cm between the potential control plates and the end wall (in a manner similar to the field line shown in Fig. 1b for the horizontal plane).

The data for Case 2 yields a more extensive point sampling over the entire machine west end wall. Three dosimeter elements are used at each location to reduce dosimetry errors. The plot for the shot-integrated x-ray intensity vs end wall position is shown in Fig. 3 as mapped to the anchor midplane. The machine operation for Case 2 was such as to only yield an average of about 4 mrem/shot, at the Case 1 access door location (and only $\sim$1.1 mrem/shot at locations behind the 7.3-cm-thick wall) for the 10 good shots of this exposure. However, this much lower x-ray intensity was at an average x-ray energy of 800 keV (2). Also, the intensity symmetry was not as good as expected, but this is generally due to detailed structure-absorber differences. In any case, an additional exposure is planned before more detailed modeling is attempted. With essentially all of the end fan magnetic field lines mapping to one of the five coaxial PPC plates, it is much harder to separate out the contributions of the outer halo from the central core. We did find that the East exposures for this data averaged 30% larger than the West exposures.

Finally, the x-ray intensity and average energy were unfolded for Case 1, with the expected thick-target bremsstrahlung yield, to set a lower limit on the total energy in this very energetic group of electrons and, hence, on the ECRH coupling efficiency. The mean photon energy from the thick-target x-ray yield is given as 0.84 times the electron energy.[3] The 350 keV X-ray energy of case 1 then converts to approximately 420 keV electrons. Also the conversion efficiency for the thick-target bremsstrahlung is given as:[4] $\eta = 1.2 \times 10^{-9} Z (V + 16.3 Z)$,

where Z is the atomic number of the absorber and V is the electron energy/e in volts. For 420 keV electrons incident on stainless steel this gives η = 1%. The data log for TMX-U includes the total incident ECRH power in the west anchor and the duration of the pulse for each shot. The model calculation corrected for yield and attenuation then produces an implied coupling efficiency of at least 10%; considering the likely more heavily attenuated softer portions of the x-ray spectrum and lower energy ECRH electrons, the actual coupling could easily be much higher.

ACKNOWLEDGMENTS

This work was performed under the auspices of the U.S. Department of Energy by the Lawrence Livermore National Laboratory under contract number W-7405-ENG-48.

REFERENCES

[1]Grubb, D. P. et al., "Thermal-Barrier Production and Identification in a Tandem Mirror," Phys. Rev. Lett. 53, 783 (1984).

[2]Homann, S., Lawrence Livermore National Laboratory, Livermore, CA, private communication (June 1984).

[3]Stallard, B. and Stephens, L., Analysis of X-ray Production in TMX-Upgrade, Lawrence Livermore National Laboratory, Livermore, CA, UCID-19313 (1982).

[4]Condon, E., Handbook of Physics, 7-119, Condon and Odishaw, Eds., McGraw Hill, N.Y. (1958).

4507v/MM

FIGURE CAPTIONS

Fig. 1. Detail of the TMX-U end tank geometry. (a) Shows a partial top view. Note the relative locations of the access port and film cassette. (b) Shows a front view. Note both the upper and lower film cassette position are shown.

Fig. 2a. Comparison of x-ray yield vs Y for X = 85 cm.
(—— ·· ——) Experimental data behind 1/16 in. Cu filter.
(————————) Normalized x-ray yield from source model shown.
(··········) Model source function (Arb. units).

2b. Same data compared with source model with no PPC plate contribution.

Fig. 3. The x-ray intensity in mrem integrated over 10 good shots as measured on the dosimeter array of Case 2 on the TMX-U end wall and projected back along field lines to the midplane of the anchor. The values enclosed by <..> below the axis correspond to correcting the intensity above, measured behind the 2.54 cm door, to the general 7.3 cm wall thickness. In general, variations >30% are due to structural features having different attenuation, though top and bottom appear distinctly higher than the two sides.

Osher, Fabyan - Figure 1

(a)

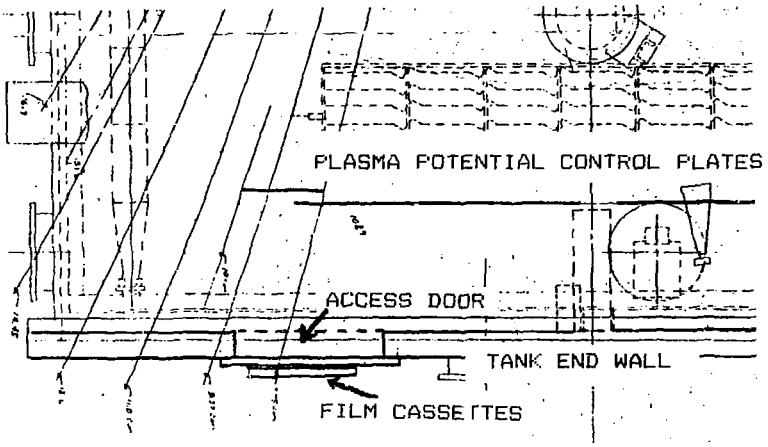

(a) Top View
(b) Front View

(b)

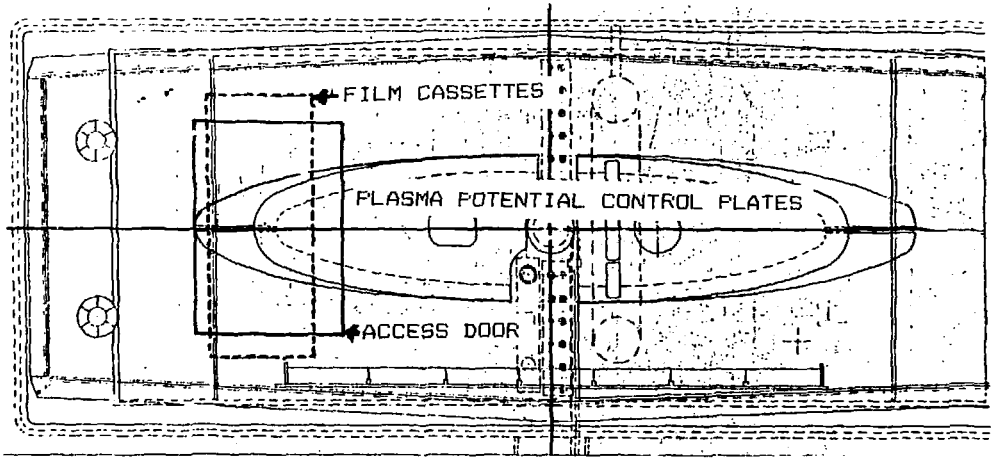

Osher, Fabyan - Figure 2

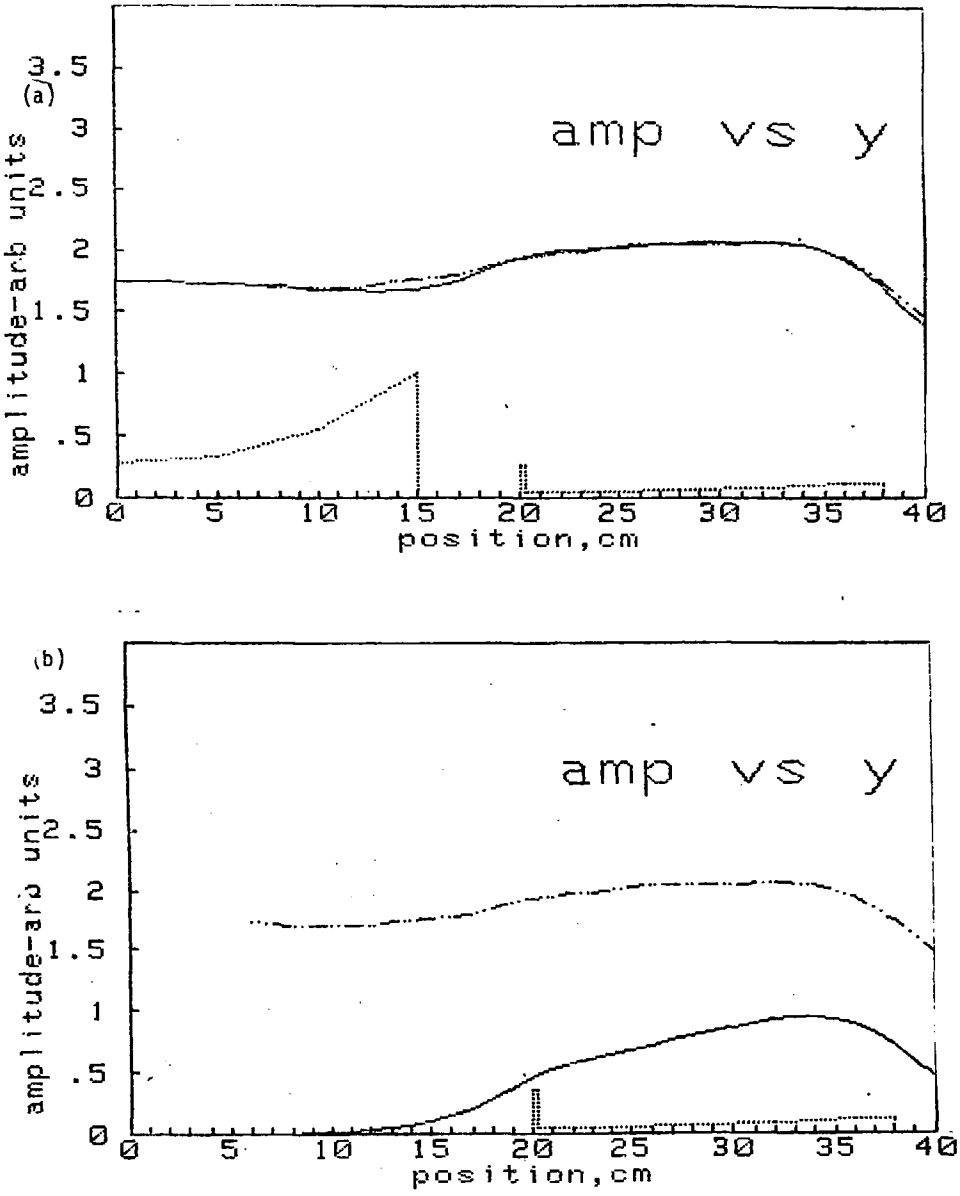

Osher, Fabyan - Figure 3